NASA TECHNICAL MEMORANDUM

NASA TM X- 68250

NASA TM X- 68250

REMOTE MEASUREMENT OF ATMOSPHERIC TEMPERATURES BY RAMAN LIDAR

by Jack A. Salzman and Thom A. Coney
Lewis Research Center
Cleveland, Ohio

TECHNICAL PAPER proposed for presentation at
Fifth Conference on Laser Radar Studies of the
Atmospheric sponsored by the Group on Laser Atmospheric Probing,
American Meteorological Society in cooperation with the
Optical Society of America
Williamsburg, Virginia, June 4-6, 1973

REMOTE MEASUREMENT OF ATMOSPHERIC TEMPERATURES BY RAMAN LIDAR

by

Jack A. Salzman and Thom A. Coney
National Aeronautics and Space Administration
Lewis Research Center
Cleveland, Ohio

ABSTRACT

The Raman shifted return of a lidar system has been utilized to make atmospheric temperature measurements. The measurements were made along a horizontal path at temperatures between -20° and +30° C and at ranges of about 100 meters. The temperature data were acquired by recording the intensity ratio of two portions of the rotational Raman spectrum which were simultaneously sampled from a preset range. Measurements were made to an accuracy of ±3° C with 1 minute temporal resolution.

E-7507

INTRODUCTION

The current interest in the environment and its conservation has resulted in considerable effort being directed toward the development of methods of measuring the many environmental parameters in question. One field of techniques being widely researched involves variations of the basic light detection and ranging (lidar) system. For example, Cooney (ref. 1) suggested that a lidar system based on Raman scattering could be used to remotely measure atmospheric temperature profiles on a real-time basis. The Raman shifted return from a number of atmospheric constituents has already been measured with a lidar system by Melfi (ref. 2) and Leonard (ref. 3) among others. Also, Coney and Salzman (ref. 4) have demonstrated that the rotational Raman spectrum of ambient air can be used to measure its temperature under laboratory conditions.

This report presents a discussion of the use of Raman scattering to remotely measure atmospheric temperatures in the field with a lidar system. The measurements were made along a horizontal path at temperatures between -20° and +30° C and at ranges of about 100 meters. The temperature data were acquired by recording the intensity ratio of two portions of the Raman spectrum which were simultaneously sampled from a preset range. Tests were initially conducted at ambient conditions utilizing the normal outside air temperature as a test parameter. Later tests utilized a control volume of air whose temperature was varied above and below ambient to acquire temperature gradient data. These tests indicate that temperature measurements are feasible with this technique and that the temperature measurement accuracies and range resolution acquired are in agreement with predicted values for the particular lidar system used in the tests.

BASIC MEASUREMENT CONCEPT

Fundamental Raman theory is well documented. The application of this theory to the modeling of an experimental rotational Raman spectrum of air was performed by Coney and Salzman (ref. 4) among others. The two spectra shown in figure 1 were calculated using this theoretical model, each for a different air temperature. Figure 1, therefore, illustrates the spectral temperature dependence of the rotational Raman spectrum of air.

One method of measuring the air temperature from spectra such as these involves taking the ratios of the intensities of discrete lines or spectral intervals (i.e., bands of lines). The purpose in using the ratios of intensities as applied to remote sensing or lidar systems is threefold. First, because the two intensities can be measured simultaneously, high temporal resolution can be obtained and real-time temperature measurements are possible. Second, because the wavelength difference of the rotational Raman lines is very small, they are affected, to a good approximation, equally by most extraneous and uncalibrated effects such as the intervening atmospheric path transmission and the response characteristics of the detection electronics. Consequently, when a ratio is taken of intensities distributed along the spectra, these unknown factors are canceled and the result depends only on temperature. Third, the sensitivity of the measurement can be enhanced by selecting appropriate line or interval combinations. Referring to figure 1, it is apparent that an increase in the gas temperature produces a decrease in intensity for those lines having j values (where j is the rotational line number designation) between the Stokes Nitrogen $j = 8$ and the anti-Stokes Nitrogen $j = 7$ lines while all other rotational line intensities increase. Taking the ratio of the intensities of two lines or intervals, one from each of these regions, will result in an enhanced ratio variation with temperature.

Raman lidar systems are required to measure very low light levels and, therefore, are generally designed so as to maximize signal statistics. Improved statistics can result with the measurements of the light intensity of bands of lines rather than single lines. Further improvement will result with the use of optical interference filters as the means of band selection since filters facilitate the design of compact receiving optics having a high light gathering capability.

The specific transmission characteristics of the filters to be used can be chosen through an analysis of the temperature sensitivity of the filter transmitted intensity and through an analysis of the system statistics. Additionally, the filters chosen must provide a high rejection capability at the laser line wavelength. Figure 2 is a plot showing the theoretical change in the transmitted intensity resulting from a change in air temperature for various filter center wavelengths and bandwidths. These data are obtained by superimposing a simple Gaussian transmission curve onto the basic Raman rotational spectrum produced by exciting laser light of wavelength 694.3 nm (ref. 4). An estimate of the total light

intensity transmitted and, thus, the statistical error to be expected is made using Raman cross section values presented in reference 5 and the system characteristics pertinent to the lidar unit used (i.e., laser power output, receiver size, etc.). This estimate is used to normalize the calculated transmissions.

The best filter combination is that resulting in the lowest statistical error and the highest temperature sensitivity. That combination exists when both filters transmit in appropriate regions of the Stokes spectrum. The final selection of filters must be made on the basis of secondary factors such as practicality of manufacture as well as on the above results.

TEST FACILITY AND LIDAR SYSTEM

Lidar Test Range

In order to evaluate the potential of a Raman lidar system and to acquire field test data with such a system, a lidar test range was constructed at the Lewis Research Center. This test range encompasses a total horizontal path length of 200 m and consists of the three major components shown in figure 3. A trailer houses the basic lidar system, associated alignment gear and other test and control equipment. Located 100 meters from the trailer is a control zone which contains a test volume of air, the temperature of which can be either raised or lowered with respect to the ambient outside temperature. Located 200 meters from the trailer is an energy dump and safety shield which terminates the laser beam's path and satisfies other safety requirements.

An interior view of the lidar trailer is shown in figure 4 locating the various control and electronic assemblies. All the test operations are controlled from this trailer compartment and all range personnel remain in this area during testing. The laser and receiving telescope are separated from this compartment by an opaque wall for reasons of safety and for isolation of the detected light from normal trailer lighting. Prior to each test shot a small hatch is opened in the front of the trailer through which the laser light pulse can exit and the scattered light can enter.

The control zone shown in figure 3 is 2.4 meters in diameter and 12 meters in length. With the end doors in the closed position the temperature of the air inside can be raised through the use of infrared heaters or cooled through the use of a liquid nitrogen heat exchanger and circulation system. The maximum attainable temperature differences or gradients are $+15^{\circ}$ and -25° C relative to the ambient air temperature. The maximum positive temperature gradient is due simply to a limitation of heater power. The maximum negative temperature gradient is dictated by the increasing potential for fog generation at larger gradients. A series of thermocouple rakes is used to continuously monitor the air temperature and when the desired air temperature is achieved the hinged doors at each end of the zone are opened and testing can be initiated. A

0.6 meter wide collar is positioned at each end of the zone (visible in fig. ") to restrict air flow in or out of the zone. This collar then provides a 1.2 meter diameter aperture through which the laser pulse can enter and exit the control zone.

After traversing the control zone, the path of the laser pulse is terminated at the energy dump shown in figure 6. To prevent high intensity reflection, both for the protection of area personnel and the detection electronics, the energy dump is constructed from a double row of light absorbing cones set in a 1.2 meter square array. This energy dump is then backed by a large flat black screen (fig. 6) to prevent any laser light around the perimeter of the beam from proceeding down range.

Raman Lidar Unit

A schematic of the optical design of the lidar unit is shown in figure 7. The transmitter which supplies the incident light is a Q-switched ruby laser operating with an output wavelength of 694.3 nanometers. The output pulse width is 20 nanoseconds, and the output energy is 4 joules per pulse at the rate of 10 pulses per minute. The light scattered from the pulse as it passes through the atmosphere is collected by an f/13 Schmidt-Cassegrain telescope 25.4 centimeters in diameter. Because of the short ranges involved in this testing, the optical axis of this telescope is aligned to intersect the path of the light pulse at a range of 100 meters.

Light collected by the telescope is passed to an optics box where it is first split into two components by a pellicle beam splitter with each component then going to a filter-detector assembly. These filter-detector assemblies (i.e., filter 1-PMT 1 and filter 2-PMT 2 in fig. 7) supply the Raman intensity data used in the temperature measurement. The temperature of these filters is controlled to maintain their measured transmission characteristics and the gain of the PMT's are periodically monitored using a light emitting diode-fiber optic unit. A portion of the combination Rayleigh-Mie scattered light at 694.3 nm which is rejected and, thus, partially reflected by filters 1 and 2 is monitored using the filter 3-PMT3 assembly.

The transmission characteristic of the two Raman filters were originally chosen on the basis of the theoretical analysis presented earlier, i.e., transmitting in the Stokes region of the spectrum. However, when these filters were used, a laser line rejection significantly poorer than that measured in the laboratory was experienced. It was concluded that this extra "leakage" was due to stray 694.3 nm light in the optics unit which was reflected onto the filters at a high angle of incidence. Because the center wavelength of a filter shifts toward shorter wavelengths as a function of angle of incidence, the laser line rejection was effectively degraded.

To alleviate this difficulty, the previous filter selection analysis was used to reevaluate the optimum filter combination with consideration

given to the anti-Stokes spectrum only. (The use of filters transmitting at the shorter anti-Stokes wavelengths also had the advantage of providing better rejection of light scattered by fluorescence.) The final filter combinations which were used to obtain the data in this report consisted of a pair of ganged filters in each of the two Raman channels. The center wavelength and bandwidth of each filter in the one pair was 691.4 and 0.6 nm, respectively, and in the other pair was 687.5 and 3 nm, respectively.

The signal outputs of the three filter-PMT assemblies are sent to an electronics unit for processing and display (fig. 8). The Rayleigh-Mie signal is simply displayed on an oscilloscope. The Raman signals are also sent to an oscilloscope display but in addition they are processed for a more accurate read-out and storage. A 20 nanosecond segment of the total return signal is sampled during each test. The relative time at which this sample is taken after the laser firing determines the range from which the scattered light is being detected. The time synchronization for this sampling is provided by a signal pulse from the laser Q-switch.

The time or range at which the sample is taken can be continuously adjusted from about 80 to 200 meters. The signal is sampled and gated using a standard nuclear instrumentation module called a "linear gate and hold" by its manufacturer. This gate has a 100-megahertz analog bandwidth and a combined gate opening and closing time of 5 nanoseconds. The gate output is integrated and held such that the magnitude of the output is a linear function of the integral of the signal during the gate opening. Because the output is held for 500 microseconds it can be digitized by moderate-speed commercial analog-to-digital converters for display on a light-emitting-diode numeric array and for storage on printed tape. A more detailed description of these detection electronics can be found in reference 6.

TEST RESULTS

If the signal outputs of the three filter-PMT assemblies are displayed on an oscilloscope, the resulting voltage traces are as shown in figure 9. The waveforms represented in this figure were traced from high-speed polaroid photographs and, therefore, are representative of the shapes and signal-to-noise ratios which were actually received. The vertical scales of the two Raman channels are the same and their intensities can be compared directly. The intensity scale of the Rayleigh-Mie channel, however, is arbitrary because of the secondary nature of its signal acquisition. Only qualitative measurements are possible with this signal. The actual Rayleigh-Mie scattered light intensity is at least three orders of magnitude greater than the Raman intensity.

In each of the traces in figure 9, at time or range equal to zero the light pulse leaves the laser and the intensity level is that of the electronic baseline. Tests were conducted during both daylight and nighttime hours and in all cases the background level due to ambient light in-

tensities was within the noise level of the system. This complete lack of background ambient light can be attributed in part to the horizontal beam path and the terminating energy dump but no tests were made to evaluate the effects of these constraints. After the light pulse leaves the laser, the received signal starts to increase until it reaches a maximum at that range where the beam path is fully within the field-of-view of the receiver telescope. After this full-cut-on point the mean return signal decreases as the inverse square of the range. The increased signal at a range of 200 meters represents a reflection from the energy dump.

After the full-cut-on point, the ratio of the intensities of the two Raman channels at any particular range is a direct indication of the atmospheric temperature at that range. While traces such as these could be used to make quantitative temperature measurements and perhaps also to determine temperature gradient locations, the accuracy of this data reduction procedure is severely limited and when using common manual techniques the data acquisition rate is slow.

Temperature measurement data obtained in digital format is shown in figure 10 where the measured Raman intensity ratio is plotted as a function of the ambient atmospheric temperature. The control capabilities of the control zone were not utilized for these tests. These data samples were taken at ranges varying from about 100 to 120 meters on days during the winter months when the ambient temperature was in the range from -10° to $+15^{\circ}$ C. Each data point on this plot represents the arithmetic average of 10 test shots or 1 minute of test time.

The line shown in figure 10 is a least squares fit to the data and is essentially a calibration curve of the system. From data such as this the variation in the ratio of the Raman intensities with temperature can be established for the particular optical and filtering arrangement employed in the system. The temperature measurement accuracy of this system can be defined by the one-standard-deviation of the data from the calibration line. This deviation was $\pm 3.3^{\circ}$ C.

Having determined the system calibration, additional tests were conducted using the control zone to create a temperature gradient in the beam path. Figure 11 shows the results of the tests where again each data point represents the average of 10 test shots. For these tests, the sample range was centered in the control zone. The predicted ratio variation with increased or decreased zone temperature was determined from the calibration test data. The mean zone temperature for the series ranged from 15° C above ambient to 25° C below ambient. In general, the greatest error from predicted behavior was because the measured deviation was not as large as that expected. This could be because the differential between the sampled air volume temperature (measured by thermocouple probes) and the ambient air temperature was really not as large as indicated. The actual temperature of the air inside the zone could normally only be determined to within about 5° C before the test shots due to uneven heating or cooling and ther-

mal stratification and to within about 8° C after the test shots due to migration of ambient air into the zone. Also, any error in establishing the range at which the sample was taken would cause deviation in the temperature of sample volume toward ambient. The results shown in figure 11 do indicate that a temperature gradient of less than 12 meters can be detected by the system.

A number of similar zone tests are shown in figure 12 in a different format. The solid circles represent the lidar temperature measurement data (i.e., from 10 test shots) giving the temperature measured and the range at which the measurement was made. The solid lines represent the actual temperature of the air. The temperature measurement between the ranges of 98 and 110 meters (i.e., within the control zone) were made using thermocouples. The shaded area shows the uncertainty in this baseline measurement. The temperature on either side of this range segment is the ambient outside air temperature of the day.

Test No. 1 indicates that there are no range effects nor any contribution to the lidar measurement due to the presence of the control zone. For this test the temperature of the zone was allowed to stabilize to that of the outside air. Both lidar measurements of the air temperature compare well with the actual outside temperature.

Tests Nos. 2 and 3 show the lidar measured temperatures for zone temperatures elevated about 15° C above ambient. The ambient air temperature was 0° and +15° C, respectively. In both tests, a lidar measurement of the ambient air temperature was made at a range beyond the zone of warm air with no degrading effects. Test No. 3 is an example of the system's range resolution. The ambient measurement was made only 6 meters from this zone of warm air.

Concurrent with the acquisition of the temperature gradient or control zone data presented in figures 11 and 12, periodic checks of the reproducibility of the calibration data of figure 10 were made. Prior to the completion of this control zone test series no inconsistencies were noted. Approximately one month after the completion of that series, a second calibration series was conducted. These new data agreed with the previous calibration data in the low temperature region but the measured intensity ratio was consistently lower in the high temperature region. This deviation reached 20 percent at 20° C.

After additional testing it was concluded that there had been a permanent shift in the calibrated sensitivity of the system. It is believed that this shift was caused by a change in the transmission characteristics of the filters which in turn was caused by extreme heat cycling of the trailer interior during the period between the two test series. This observed shift in the calibration curve of the system indicates that although relative temperature measurements can be made quite easily with the present system, absolute temperature measurements will either require repeated calibration checks or upgraded system capabilities.

CONCLUSION

In summary, it may be stated that the Raman shifted return of a lidar system can be utilized to make atmospheric temperature measurements. For the lidar system tested, the accuracy of these measurements at a range of 100 meters is $\pm 3^{o}$ C with 1 minute temporal resolution. Because this measurement accuracy compares well with that predicted for this particular unit, it is suggested that a field-application system could be built with significant improvements in both absolute accuracy and range.

REFERENCES

1. Cooney, J., 1967: Satellite Observation Using Raman Component of Laser Backscatter. Proceedings of the Symposium of Electro-Magnetic Sensing of the Earth from Satellites. Polytechnic Institute of Brooklyn Press, pp. P1-P10.

2. Melfi, S. H., 1972: Remote Measurements of the Atmosphere Using Raman Scattering. Appl. Opt., 11, 1605.

3. Leonard, D. A., 1972: Using Lasers to Monitor Stack Emissions. Instr. Control Systems, 45 (8), 73.

4. Coney, T. A., and Salzman, J. A., 1973: Determination of the Temperature of Gas Mixtures by Using Laser Raman Scattering. NASA TN D-7126.

5. Penney, C. M., St. Peters, R. L., and Lapp, M., 1973: Absolute Intensity and Polarization of Rotational Raman Scattering from N_2, O_2, and CO_2. General Electric Co., SRD-72-163, NASA CR-121091.

6. Leser, R. J., and Salzman, J. A., 1972: Light Detection Electronics for a Raman Lidar. NASA TN D-6879.

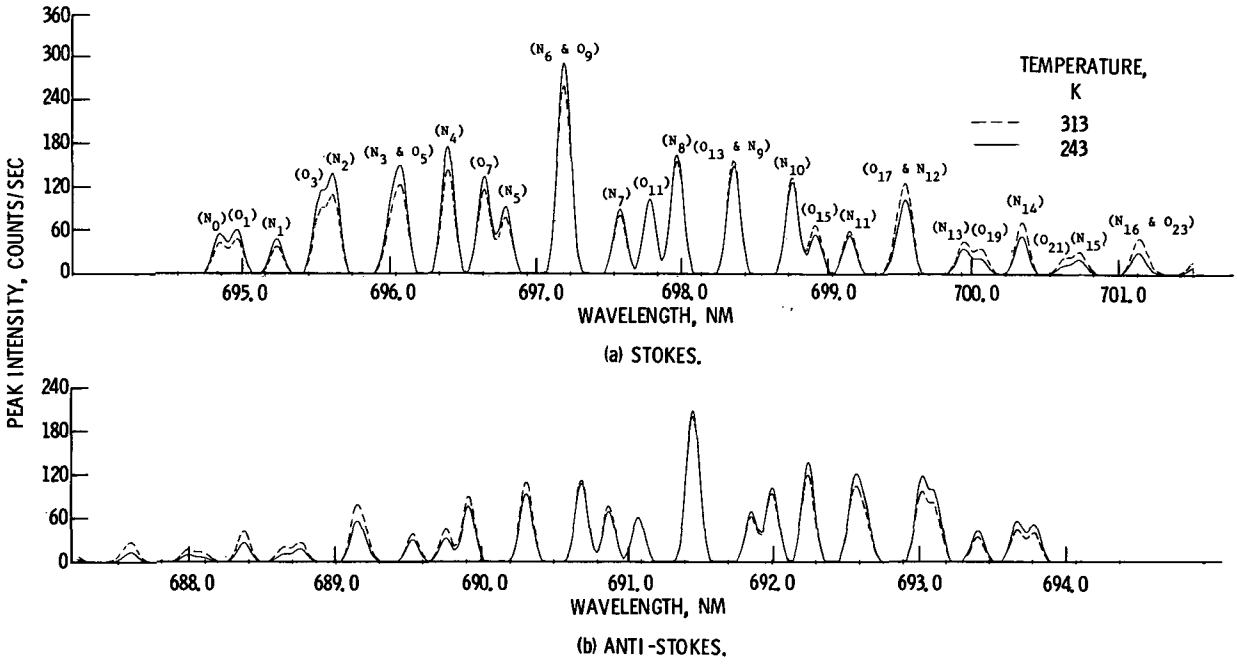

Figure 1. - Comparison of theoretical spectrum of air for temperatures of 243 and 313 K.

E-7507

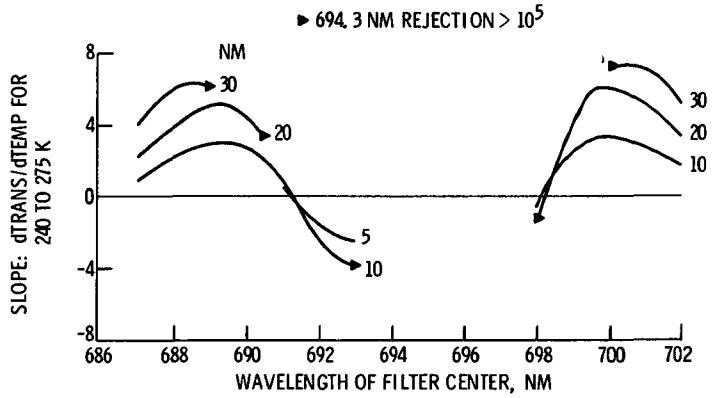

Figure 2. - Filter characteristics determining optimum temperature measurement sensitivity.

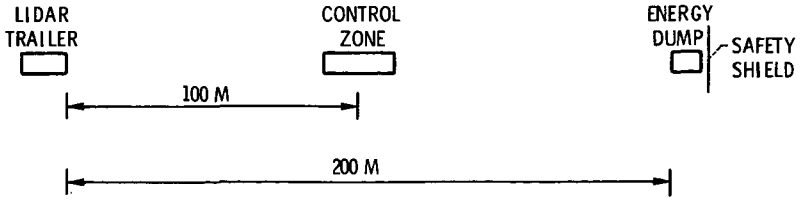

Figure 3. - Lidar test area.

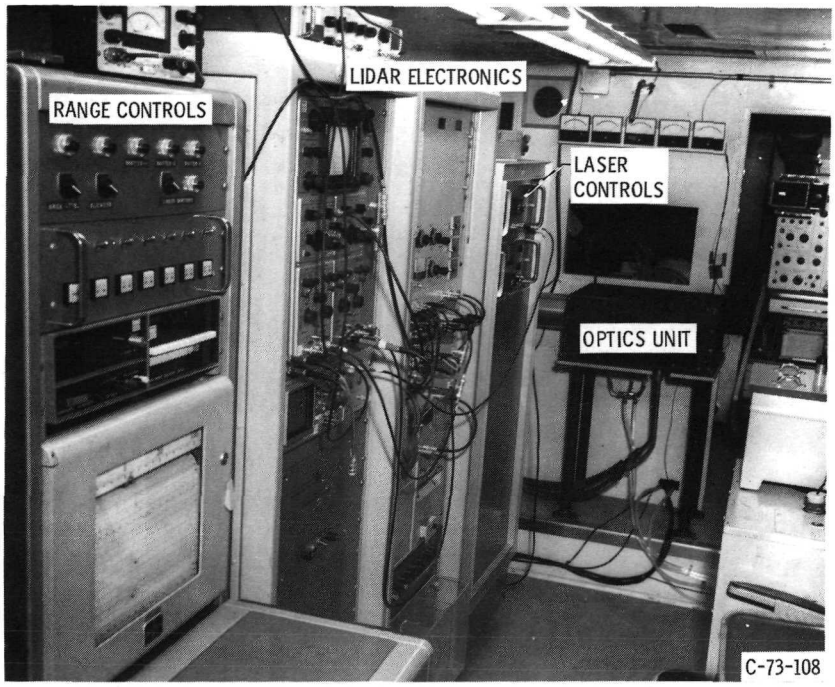

Figure 4. - Interior of Lidar trailer.

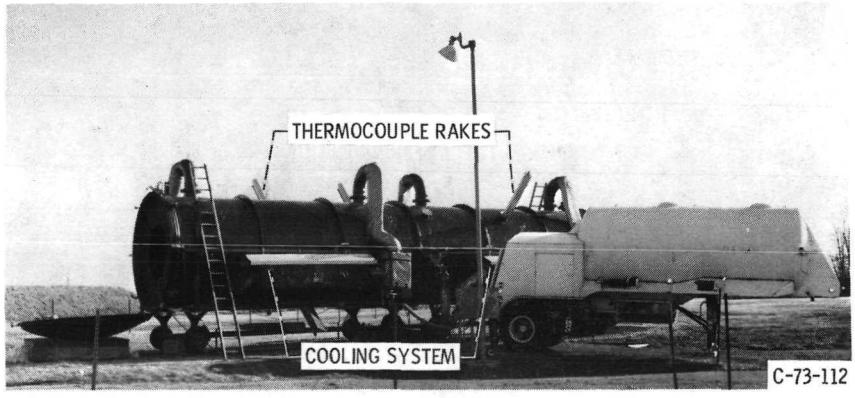

Figure 5. - Temperature control zone.

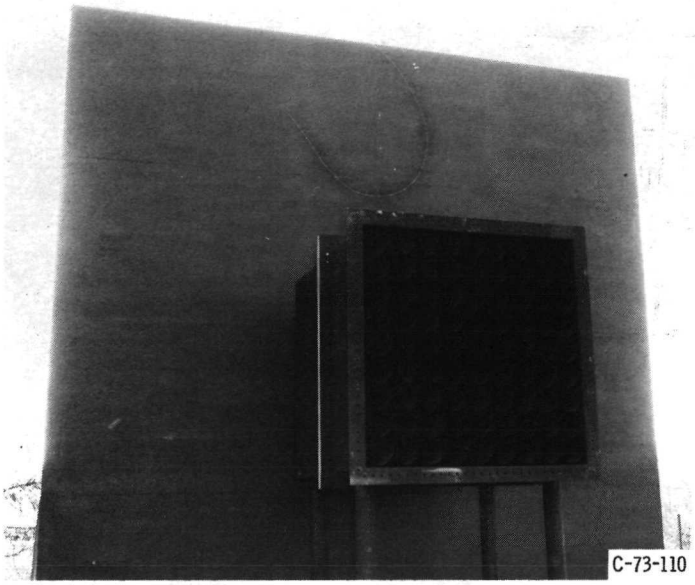

Figure 6. - Energy dump and safety shield.

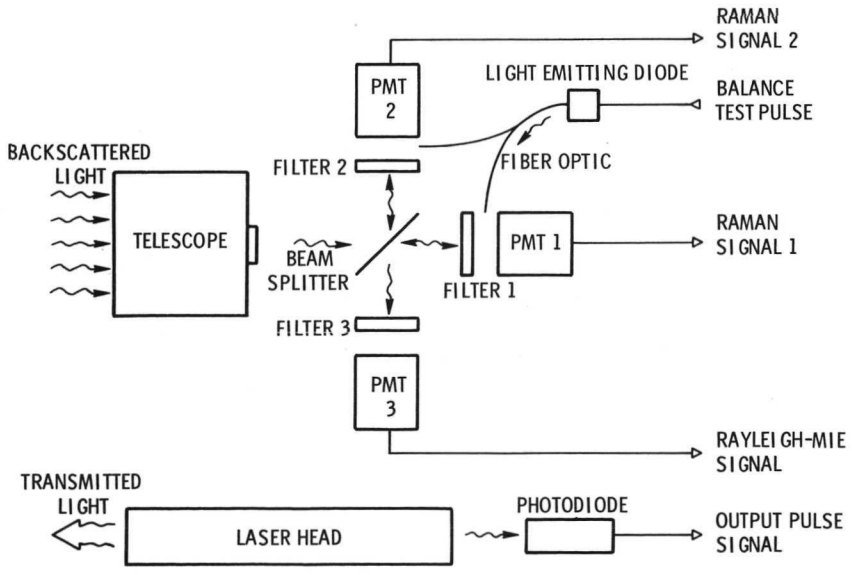

Figure 7. - Optical design schematic.

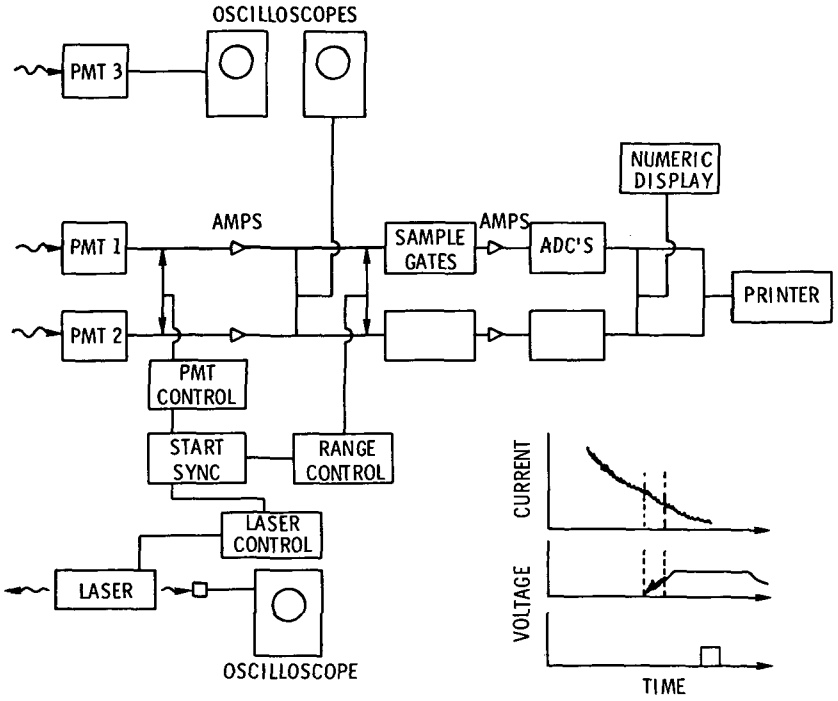

Figure 8. - Block diagram of Lidar Electronics.

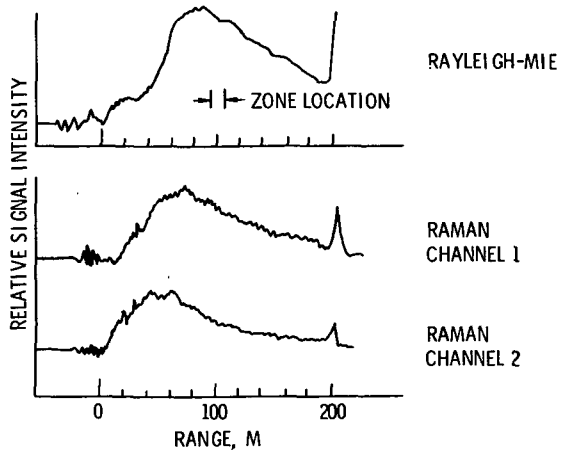

Figure 9. - Typical analog return signals.

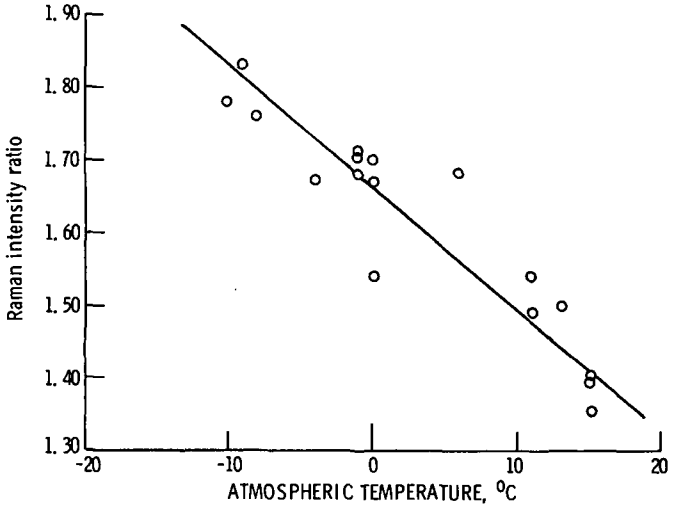

Figure 10. - Variation of Raman intensity ratio as a function of ambient atmospheric temperature.

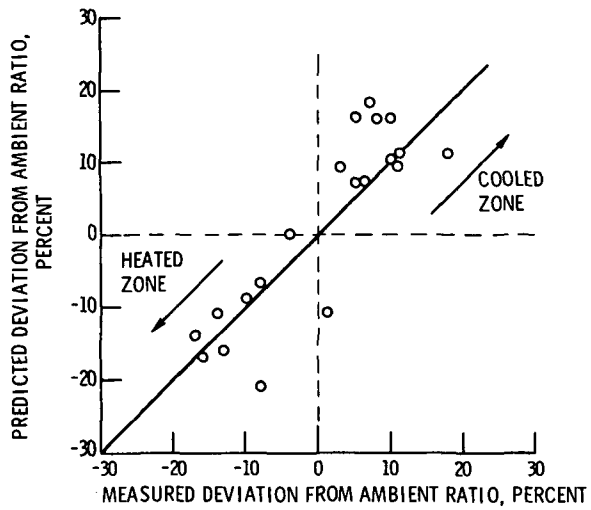

Figure 11. - Deviation in Raman intensity ratio for zone temperature above and below ambient.

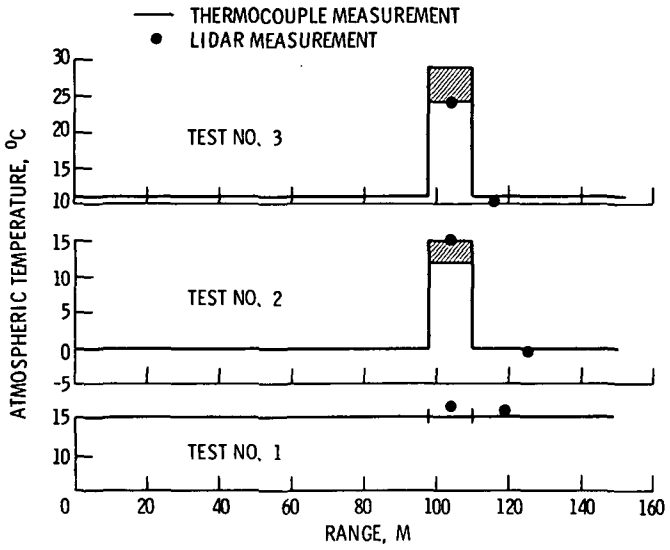

Figure 12. - Temperature gradient measurements.